Investigate the potential of using reactor anti-neutrinos for nuclear safeguards in Vietnam

S. Cao[1], **T. V. Ngoc**[1,2], **N. T. Hong Van**[3] **and P. T. Quyen**[1]

[1]*Institute for Interdisciplinary Research in Science and Education, Quy Nhon, Vietnam*

[2]*Graduate University of Science and Technology, Vietnam Academy of Science and Technology, Hanoi, Vietnam*

[3]*Institute of Physics, Vietnam Academy of Science and Technology, Hanoi, Vietnam*

E-mail: †cvson@ifirse.icise.vn

Abstract. *One of the most abundant man-made sources of low energy (few MeVs) neutrinos, reactor neutrino, is not only useful for studying neutrino properties, but it is also used in practical applications. In this study, we investigate the potential of using reactor neutrino detectors for nuclear safeguards in Vietnam, specifically at the Dalat Nuclear Reactor, a future research facility, and presumably commercial reactors with 500 kW, 10 MW, and 1000 MW thermal powers, respectively. We compute the rate of observed inverted beta decay events, as well as the statistical significance of extracting isotope composition under the practical assumptions of detector mass, detection efficiency, and background level. We find that a 1-ton detector mass can allow us to detect the reactor's on-off transition state from a few hours to a few days, depending on the standoff distance and reactor thermal power. We investigate how background and energy resolution affect the precision of the extracted weapon-usable ^{239}Pu isotope. We conclude that in order to distinguish the 10% variation of the ^{239}Pu in the 10 MW thermal power reactor, a 1-ton detector placed 50 m away must achieve 1% background level. Increasing the statistics by using a 10x larger detector or placing it $\sqrt{10}$ times closer to the reactor alleviates the requirement of the background level to 10%.*

Keywords: vietnam reactor; neutrino detection; safeguard; Pu isotop.

Classification numbers: 14.60.Lm; 14.60.St.

1. **Applied anti-Neutrino detection: a "ghost" particle for peace**

In 1930, W. Pauli [1] proposed the existence of neutrino –a neutral lepton particle –to address the continuity of the beta decay spectrum, and it was experimentally detected for the first time in a reactor-based experiment twenty-six years later [2]. The neutrino interacts only weakly in the Standard Model of elementary particles and is predicted to be massless because only left-handed neutrinos have been observed experimentally [3]. The fact that neutrinos are massive, as indicated by neutrino oscillations [4, 5], is experimental evidence that defies explanation by the Standard Model. Many efforts, summarized in Ref. [6], have been made over nearly a century to understand the nature of neutrinos. However, neutrinos remain one of the universe's most enigmatic particles. In fact, we still do not know whether neutrinos are Dirac or Majorana particles. We do not know how neutrinos can have an extraordinary smallness of mass, at least one million time smaller than the electron's mass. Despite some exciting hints [7], there is insufficient statistical evidence to conclude that neutrino interactions violate the charge-conjugation and parity symmetry. The current state and future prospects of neutrino physics can be found, for example, in Ref. [6, 8].

Since neutrinos interact weakly with matter, they can pass through the earth, the sun, and the stars unaffected. On the one hand, it makes neutrino detection extremely difficult. Typically we require a large detector and a powerful neutrino source to make neutrinos visible. But on the other hand, it ushers in a new era of applied neutrino physics with reactor non-intrusive monitoring. Neutrino emitted by a reactor is electron anti-neutrino $\overline{\nu}_e$; we will refer to it as *reactor neutrino* from now on. The reactor neutrinos are commonly detected using the inverse beta decay (IBD), which is discussed in Sec. 2. With recent advances in detection technology and our progress in understanding reactor neutrino production, we can remotely monitor reactor thermal power and measure isotope composition using neutrinos as a working tool [9]. Plutonium ^{239}Pu, one of the reactor's four main isotopes, can be used to make nuclear weapons. As a matter of fact, continuous monitoring of the plutonium content in the reactor is critical for nuclear safeguards and verification regulations.

Since the 1980s, there has been discussion [10] about the practical application of measuring reactor neutrino production to monitor the reactor itself. Further research in the 1990s and the early 2000s [11–14] confirmed the direct relationship between the reactor thermal power and the number of reactor neutrinos. To reduce background caused by the cosmic rays, the detectors, which were typically cubic meters in size, were placed a few tens of meters underground. One of the earliest efforts to realize the ground-level reactor neutrino-based monitor was developed at Japan's fast reactor JOYO [15]. However, the presence of a large background prevents this experiment from definitively reporting the reactor's on-off transition. A significant progress and now becoming a benchmark [16] for the neutrino-based reactor monitoring come from the PROSPECT experiment [17]. PROSPECT can achieve signal-to-background (S/B) ratio of 1:1 with an overburden of approximately one meter-water-equivalent (mwe). There are a large number of efforts around the world to realize this emerging neutrino-based technology, which are summarized in Table 1. The historical development of this field can be found in Ref. [9, 18]. In terms of detection technology, liquid scintillator (LS) and plastic scintillator (PS) are commonly used to detect the prompt e^+ signals produced by the IBD in conjunction with neutron. The water Cherenkov (WC) detectors with Gd-doped are occasionally chosen. There are several advantages to using

Table 1. Reactor-based projects developed in the 20th century targeting the reactor monitoring. Some projects have developed for fundamental physics for searching the sterile neutrino at very short-baseline neutrino experiment

Experiment	Country	Com. Year	Dist. [m]	Detection Specification
SONGS1 [19] SONGS [20]	US US	2003 2009	20 50	0.6-ton Gd-LS; 25 mwe overburden PS + ^{6}Li; ground-level; movable
At JOYO [15]	Japan	2007	24.3	0.76-ton Gd-LS; ground-level
Cormorad [21]	Italy	2009	25	PS w/ Gd-coated sheet
PANDA [22]	Japan	2011	36	PS w/ Gd-coated sheet; ground-level; movable
Nucifer [23]	France	2012	7	0.8-tons Gd-LS; 12 mwe overburden; PSD capability
Liverpool [24] VIDARR [25]	UK UK	2014	60 Any	1-ton PS + Gd-coated sheet; movable 1.5-ton PS + Gd-coated sheet; movable
Nulat [26]	US	2015	3-6	1-ton PS + ^{6}Li
WATCHMAN [27]	US,UK	2015	25000	1-ktons Gd-doped WC
Solid [28] ([29])	Belgium	2015 (2018)	6-9	288kg (1.6-tons) PS cube LiF-ZnS; PSD capability
DANSS [30]	Russia	2016	10.7-12.7	1-ton, PS-Gd, Movable, 50 mwe overburden
NEOS [31]	South Korea	2017	23.7	1-ton Gd-LS; 25 mwe overburden; PSD capability
MiniCHANDLER CHANDLER [32]	US US	2017	Any Any	80 kg PS + ^{6}Li; ground-level 1-ton PS + ^{6}Li; ground-level
Angra [33]	Brazil	2017	Any	1.34-ton GdCl3 WC; ground-level
STEREO [34]	France	2018	10.3	1.8-ton, segmented Gd-LS; 10 mwe overburden; PSD capability
PROSPECT [17]	US	2018	7	4-tons segmented Li-LS; ≤ 1 mwe overburden; PSD
Neutrino-4 [35]	Russia	2019	6-12	1.42m3, segmented Gd-LS; movable; $\sim$10 mwe overburden

a liquid scintillator, including high light yield, low energy threshold, homogeneity, purification, large-detector scalability, and cost-effectiveness. However, because they are highly flammable, poisonous, and chemically dissolved, LS are difficult to handle and operate. When a mobile neutrino detector for nuclear safeguards is considered, the situation becomes even more difficult. PS-based detectors have emerged as a viable option for safer above-ground deployment. Furthermore, the segmentation approach allows us to measure both the temporal and spatial correlations of the IBD-induced signal, thus enhance the S/B performance. The Gadolinium (Gd) or Lithium (Li) are normally deployed to increase the neutron-captured efficiency. Some detectors are equipped with the pulse-shape discrimination (PSD) capability to distinguish the neutron-induced signals

from the gamma background. Some have the "movable" capability, which is essential for the above-ground safeguard.

To sum it up, the technology for the neutrino-based reactor monitors is ready for the commercialization and deployment [9]. Further research is needed to refine the technology and optimize it for cost, detection efficiency, and portability. The reactor-based neutrino experiments have played important role in exploring the fundamentals of neutrino particle, including but not limited to the discovery of neutrino [2] and precision of mixing angle θ_{13} [6]. Still the medium-baseline experiment like JUNO [36] can help us to determine the neutrino mass ordering, which is one of the unanswered questions of the neutrino physics. The short baseline experiment was designed to not only provide a precise understanding of the reactor neutrino flux, but also to search for the sterile neutrino, as seen in Ref. [37]. There is a strong synergy between the applied antineutrino physics for non-destructive monitoring and the basic science research with the reactor neutrinos.

In this work, we assess the feasibility of using reactor antineutrinos for nuclear safeguards, taking into account the availability and prospects of nuclear reactor facilities in Vietnam. The paper is organized as follows. Section 2 discusses two key components that are also essential inputs for our simulation: our understanding of reactor neutrino flux and our capability for detecting reactor neutrinos while taking into account the scale of detector. Section 3 describes the status of reactor facilities in Vietnam as well as our assumptions about their thermal power for the simulation. Section 4 presents the results of the expected rate of reactor neutrinos and the time to detect the on-off transition. Section 5 focuses on the possibility of extracting the plutonium content from the measured spectra of detected reactor neutrinos. Finally we conclude our study in Sec. 6.

2. Reactor neutrino flux and detection methodology

Understanding the neutrino produced by the reactor is critical for both basic science and practical applications of the reactor neutrinos. It is recalled that reactor neutrinos are produced from the $\sim 10,000$ beta decay branches of the ~ 800 fission fragments, which are generalized with $^A_Z X \to ^A_{Z+1} X + e^- + \overline{\nu}_e$. Neutrinos are produced along with the associated beta particles. For this reason, there are two approaches for calculating the neutrino production from the reactor. The first approach is to sum up all beta-decay branches from all fission fragments. An updated summation model, called *ab initio*, can be found in Ref. [38]. The second approach is to extract the the reactor neutrino spectrum from the β-spectral measurements. For the most of commercial reactors, there are four main isotopes ^{235}U, ^{238}U, ^{239}Pu, and ^{241}Pu, which contribute to approximately 99.9% of the total reactor neutrino flux. The lifetime, natural abundance, number of reactor neutrinos per fission, and the released thermal energy per fission for individual isotopes are shown in Table 2. The β-spectral measurements for these isotopes have been carried out [41–45] and there are two

Table 2. Four main isotopes in the reactor are presented with the lifetime, natural abundance, neutrino yield, and released thermal energy. Values are based on Ref. [39, 40]

Isotope	^{235}U	^{238}U	^{239}Pu	^{241}Pu
Lifetime[year]	7×10^8	1.6×10^5	2.4×10^4	14
Natural abundance [%]	0.72	99.27	0.0	0.0
$N_{\overline{\nu}_e}$ per fission	1.92 ± 0.04	2.38 ± 0.05	1.45 ± 0.03	1.83 ± 0.03
E_{released} per fission [MeV]	201.7 ± 0.6	205.0 ± 0.9	210.0 ± 0.9	212.4 ± 1.0

neutrino flux models [46, 47] [48] based on these measurements. The comparison among these flux models can be found in Ref. [37]. The uncertainty on the integrated flux of ^{235}U, ^{239}Pu, and ^{241}Pu is about 2-3% while the uncertainty on the integrated flux of ^{238}U is about 11%. At a given time t, when the fission fraction f_i of the ith isotope and their corresponding neutrino spectrum $S_i(E_{\bar{\nu}_e})$ is known, the total reactor neutrino flux $\Phi(E_{\bar{\nu}_e}, t)$ can be summed up and normalized by the thermal power of the reactor $W_{\text{th.}}$ and the released thermal energy e_i by the isotope:

$$\Phi(E_{\bar{\nu}_e}, t) = \frac{W_{\text{th.}}(t)}{\sum_i f_i(t) e_i} \times \sum_i f_i(t) \times S_i(E_{\bar{\nu}_e}, t). \tag{1}$$

In average, as shown in Table 2, every fission releases about 200 MeV of energy and emits about 6 electron anti-neutrinos along the beta decay chain. For a reactor with 1 GW$_{\text{th.}}$ (equivalent to 6.242×10^{27} eV/s), the corresponding number of fission occur per second is computed to be 3×10^{19}(fissions). Thus, the total number of anti-neutrinos emitted by a 1 GW$_{\text{th.}}$ reactor are $\approx 2 \times 10^{20}$ particles per second. If the detector stands off at 50 m, it will receive a reactor neutrino flux of 6×10^{11} s^{-1}cm^{-2}.
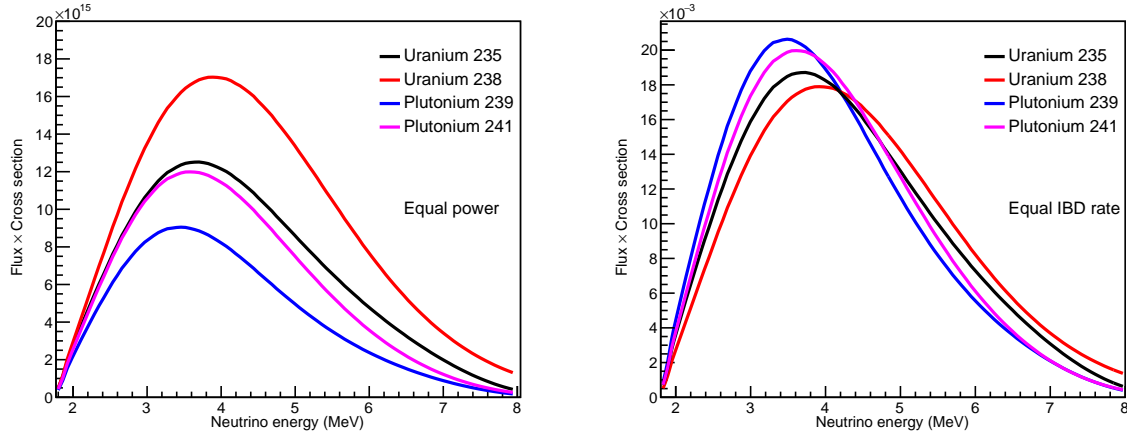

Fig. 1. Contribution to the reactor neutrino flux from four main isotopes in term of the product of flux and cross-section as a function of neutrino energy. The left plot is with equal power and the right is with equal IBD rate. The ^{239}Pu and ^{241}Pu spectra are softer than the ^{235}U and ^{238}U.

Fig. 1 shows the individual contributions from the four main isotopes to the total reactor neutrino flux. The comparison is on the product of the flux and IBD cross section and is shown in two cases (i) equal power and (ii) equal IBD rate. It can be observed that the ^{239}Pu-contributed neutrino spectra are softer than the $^{235,238}U$-contributed neutrino spectra. As a result, the overall reactor neutrino spectrum will become softer when the fraction of ^{239}Pu increases. This is a key point for using reactor neutrino as an isotope spectroscopy, which is discussed in detail in Section **5**.

The observable rate of reactor neutrino as a function of energy $E_{\bar{\nu}_e}$ and time t, $N_{\bar{\nu}_e\ det.}(E_{\bar{\nu}_e}, t)$ as shown in Eq. 2, is proportional to the reactor neutrino flux $\Phi(E_{\bar{\nu}_e}, t)$ defined in Eq. 1, detector standoff $\frac{1}{4\pi L^2}$, the cross section $\sigma(E_{\bar{\nu}_e})$, the number of targets of the detector N_{target}, the neutrino detection efficiency $\epsilon(E_{\bar{\nu}_e})$, and the survival probability of reactor neutrinos $P_{(\bar{\nu}_e \to \bar{\nu}_e)}(E_{\bar{\nu}_e}, L, \vec{o})$

where $\vec{o}$ presents the mixing parameters of the neutrino oscillation.

$$N_{\bar{\nu}_e \, det.}(E_{\bar{\nu}_e}, t) = \frac{\Phi(E_{\bar{\nu}_e}, t)}{4\pi L^2} \times \sigma(E_{\bar{\nu}_e}) \times N_{\text{target}} \times \epsilon(E_{\bar{\nu}_e}) \times P_{(\bar{\nu}_e \to \bar{\nu}_e)}(E_{\bar{\nu}_e}, L, \vec{o}). \qquad (2)$$

The IBD cross section, which is about $5 \times 10^{-43} \text{cm}^{-2}$ at 2 MeV neutrino energy, has been computed in Ref. [49] with less than 1% uncertainty. The neutrino-based reactor monitoring can be classified into two types based on the reactor-to-detector distance. For near-field ($L \sim 10s$ m) monitoring and if there is nonexistence of sterile neutrinos at eV scale, the oscillation probability can be approximated to be $P_{(\bar{\nu}_e \to \bar{\nu}_e)} \approx 1.0$. The effect of oscillation phenomenon should be taken into account with the far-field ($L \sim 10s$ km) monitoring. The IBD detection efficiency with LS-based detectors [17,29] is slightly more than 40%. For the segmented PS-based reactor mornitoring [32], the detector IBD efficiency reaches to approximately 60%. In short, a 1-ton detector, which stand off 50 m from a 1 GW$_{\text{th}}$ reactor, can detect few 10s of the IBD interactions per hour.

Although other methods, such as charged-current and neutral-current interactions with heavy waters, neutrino-electron elastic scatterings, and neutrino-nucleus coherent scattering, can be used to detect reactor neutrinos, the most common method is the aforementioned IBD, which produces simultaneously positron and neutron in the final state:

$$\overline{\nu}_e + p \to e^+ + n, \text{ (when } E_{\overline{\nu}_e} > 1.806 \text{ MeV)}. \qquad (3)$$

The spatial and temporal coincidence of the highly detectable positron and neutron provides us with a distinguishing feature that allows us to effectively identify the reactor neutrinos. The threshold of this reaction is 1.806 MeV due to the difference in the (e^+, n) mass and $(\overline{\nu}_e, p)$ mass. The spectrum of the reactor neutrinos can be deduced from the measured beta spectrum using the relation $E_\nu = E_{e^+} + 0.784$ MeV. Positron induced from the IBD quickly deposits its energy and annihilates with an electron of the medium to create two gamma rays with typical 511 keV prompt signals. Neutron can be captured by free proton or Hydrogen (H), gadolinium (Gd), or Lithium (Li) depending on the detector technology leaving a delay gamma cascade. The general principle for detecting the reactor neutrinos via the IBD reaction is illustrated in Fig. 2.

Most of the detectors developed for the safeguard purpose must be sensitive to see both the prompt signal and delay signal to identify the IBD interaction. For a particular detector, the light collection of the positron prompt signal determines the reconstructed energy resolution of the reactor neutrinos. This essentially depends on the scintillation light yield, photosensor coverage, and quantum efficiency of the photosensor. The LS-based detector can reach 1000 p.e. per 1 MeV deposition, resulting in 3-4% energy resolution at 1 MeV. The PROSPECT experiment [17] has already achieved 4.5% energy resolution while JUNO [36], a medium-baseline experiment for the basic science, can achieve 3% energy resolution. For the PS-based detector, the miniCHANDLER [32] have achieved 10% energy resolution. Signature of the neutron capture is important to discriminate the reactor neutrino events from the backgrounds. Therefore, the IBD-based detectors are normally made by proton target materials. In the detector medium, neutron can be captured by a free proton or Hydrogen and subsequently produces an averaged 180 μs delayed signal of 2.2 MeV gamma ray:

$$n + p \to d + \gamma \, (2.2 \text{ MeV})$$

To increase the neutron-captured efficiency and shorten the delayed time, Gd is customarily loaded into the detector. Neutron is captured by Gd to produce 8.0 MeV gamma cascade with averagely
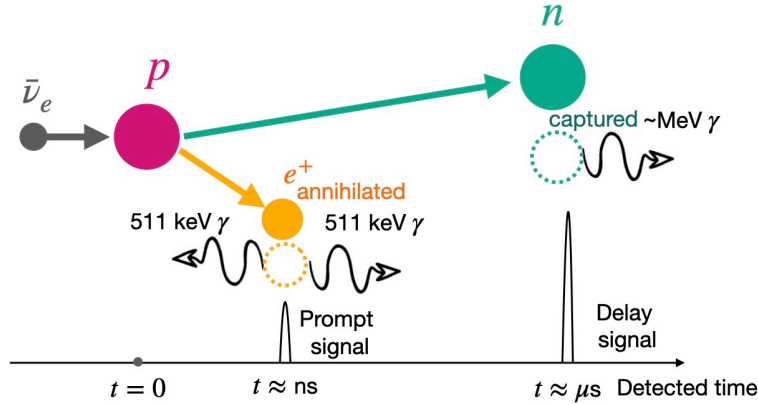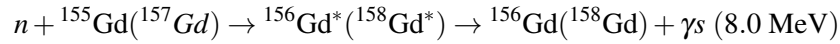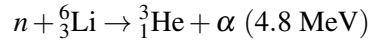
Fig. 2. Principle of the reactor neutrino detection via the inverse beta decay. A prompt signal comes from e^+ annihilation and a delayed signal is from the neutron capture. The gamma energy due to the neutron capture can be around 2.2 MeV in hydrogen or 8.0 MeV (4.8 MeV) with Gadolium (Lithium) respectively. Coincidence of the prompt signal and delay signal in a pre-defined timing window is a signal of the IBD interaction.

20 μs delayed from the prompt e^+ signal.

$$n + {}^{155}\text{Gd}({}^{157}Gd) \rightarrow {}^{156}\text{Gd}^*({}^{158}\text{Gd}^*) \rightarrow {}^{156}\text{Gd}({}^{158}\text{Gd}) + \gamma s \text{ (8.0 MeV)}$$

In the case of ${}_3^6\text{Li}$, neutron-capture process emits a 4.8 MeV α particle.

$$n + {}_3^6\text{Li} \rightarrow {}_1^3\text{He} + \alpha \text{ (4.8 MeV)}$$

The α ionization produces a relatively slow scintillation light. A detector with the PSD capability allows us to distinguish this neutron-captured signal from the huge amount of swift gamma-induced signal. The neutron-captured efficiency can exceed more than 70% [17, 29, 32]. The overall IBD detection efficiency can reach to approximately 60%.

As illustrated in Sec. 4 and Sec. 5, not only is signal detection improved, but background suppression is critical for the neutrino-based reactor monitor. Due to detector size requirements and budget constraints, active shielding is limited. Passive shielding with multi-layers of neutron-absorbing materials is widely used. One recent benchmark [17] established a signal-to-background ratio of 1:1. Advancing reactor neutrino detection and shielding technology is required to go beyond this benchmark.

3. Reactor in Vietnam and experimental simulation

Vietnam currently has only one small research nuclear reactor with a nominal power of 500 kW, the Dalat Nuclear Research Reactor (DNRR) [50], which has been operational for 60 years. DNRR has been used for neutron scattering, neutron activation analysis, material testing, medicine application, and biological science research, education, and training [51–53]. Since 2011, DNRR has been fully operating with the Low Enriched Uranium (LEU) fuel of 19.75% ^{235}U at 500 kW power. However, due to its low power and facility limitations, this research reactor will be unable to meet the increasing demands of research and application in the future. In the near

future, another 10 MW nuclear reactor for multipurpose research (MPRR) [51] is planned to be built. Aside from traditional applications, MPRR is being developed for advanced research and applications such as neutron transmutation doping of silicon and neutron scattering material science research. According to a government plan [54] approved in 2007, 8 GW$_e$ (gigawatt electrical[1]) nuclear power should be available by 2025. By 2030, the power is expected to increase to 15 GW$_e$ with a total of 14 nuclear reactors. However, the National Assembly of Vietnam postponed the plans in 2016 due to rising costs and safety concerns. Vietnam's nuclear program was recently revived and is being considered for recovery in 2022. In this work, we assume a commercial reactor (CNR) with an average thermal power of 1000 MW for study.

In this study, the General Long Baseline Experiment Simulator (GLoBES) [55] is used to simulate the reactor neutrino source and the detector setup. The inputs for GLoBES are provided including reactor and detector information as follows. For the reactor, thermal powers are 500 kW, 10 MW and 1000 MW for DNRR, MPRR, and CNR, respectively. The flux and cross section spectra are parameterized as in [40, 49]. The energy window is selected in a range from the threshold 1.8 MeV to maximum 8.0 MeV. The detector is made from plastic scintillator with total target mass of 1 ton. The signal efficiency is considered to be either 11.6% or 60%, which are based on the previous achievements in Ref. [22] and Ref. [32] respectively. There is no background specified in the simulation for simplicity. However, background is taken into account when exploring the physical potentials of the monitor. The detector setup is summarized as in Table 3.

Table 3. Nominal experimental configuration for simulation of the neutrino-based reactor monitor presented in this study.

Detector Mass	Operation Time	$\bar{\nu}_e$ energy window	Signal efficiency
1 ton	1 year	1.8 MeV - 8.0 MeV	11.6% - 60%

4. Expected rate of reactor neutrinos and time to on-off transition detection

Firstly, we investigate the number of observable events at various distances for each reactor. Fig. 3 shows the total number of observable anti-neutrino events in one year with respect to (a) the neutrino energy and (b) the distance from the reactor core. The magenta, blue and red lines correspond to 500 kW DNRR, 10 MW MPRR and 1000 MW CNR respectively. The solid lines represent 60% detection efficiency while the dashed lines are for 11.6% efficiency. It can be seen from the Fig. 3 that the observable anti-neutrino spectra are maximal at around 4 MeV energy and inversely proportional to the distance square as described in Eq. (2). Table 4 summarizes the expected annual IBD event rate at various baselines (5m, 10m, 20m, 50m). There are two numbers for the IBD event rate for each experimental configuration, which correspond to 11.6% and 60% detection efficiency, respectively. If the 1-ton detector is placed less than 20m from the DNRR reactor core, the expected IBD event rate is in the hundreds to thousands per year. The expected IBD event rate for the MPRR and CNR can reach 10^6 collected per year.

Assuming the signal-to-background (S/B) to be 1:1, achieved with PROSPECT [17], to detect the on-off transition of the reactor state at 5σ confidence-level (C.L.) statistical significance,

---

[1]GW$_e$ refers to the electric power produced by a generator. Reactor neutrino flux is proportional to the reactor thermal power, but not electrical power.
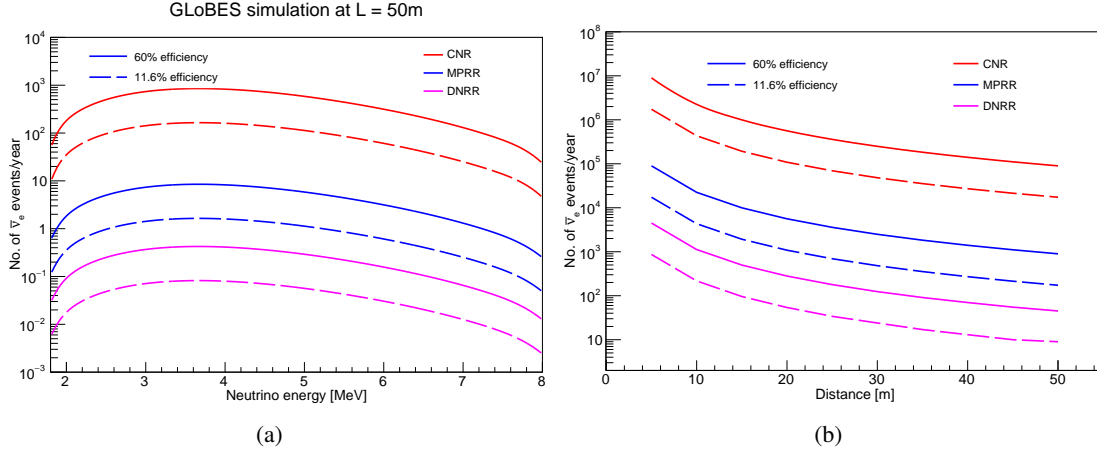
Fig. 3. (Color online) The number of electron anti-neutrino events per year as a function of the (a) neutrino energy and (b) distance from the reactor core for DNRR (magenta line), future MPRR (blue line) and CNR (red line). Solid lines and dashed are corresponding to 60% and 11.6% detection efficiencies.

Table 4. The expected IBD event rates from DNRR, MPRR and CNR at various baselines (5 m, 10 m, 20 m, 50 m) in one year. Two values in each cell are corresponding to the detection efficiencies of 11.6% and 60%.

Events/year	L=5 m	L=10 m	L=20 m	L=50 m
DNRR	867 - 4487	217 - 1122	54 - 280	9 - 45
MPRR	17349 - 89734	4337 - 22433	1084 - 5608	173 - 897
CNR	1.7×10^6 - 9.0×10^6	433714 - 2.2×10^6	108426 - 560826	17346 - 89720

the number of IBD events needed to collect is more than 30 events. The time to detection of the on-off transition state of the reactor can be calculated and shown in Table 5. It has been observed

Table 5. Time to detection of the on-off transition of the reactor state with 5σ C.L for various experimental configurations. The detection efficiency is assumed to be 60%, and S/B = 1:1.

Events/year	L=5 m	L=10 m	L=20 m	L=50 m
DNRR	2.5 days	10.1 days	40 days	251 days
MPRR	3hrs	12 hrs	2 days	12.6 days
CNR	1.8 mins.	7.4 mins.	29 mins.	3 hrs

that detecting the on-off transition of the reactor state with the DNRR takes a few days to a month if the 1-ton detector is located less than 20 m. The MPRR and CNR can detect this change in a matter of hours to days, even if the detector is placed 50 m away from the reactor core. For CNR, the time can be less than a half hour if the detector is placed within 20 m of the reactor core. The

conclusion holds if we can achieve approximately 60% IBD detection efficiency and a S/B ratio of around 1:1 or better.

5. Potential to extract the plutonium content

To extract the isotope content, particularly the nuclear weapon-usable ^{239}Pu, we rely on the reconstructed neutrino energy spectrum. Here, a 15% energy resolution is assumed without further mention throughout the work. The PS-based detector [32] can achieve 10% energy resolution while the LS-based detectors [17] can achieve 5% energy resolution. For this particular study, we assume to take a 1-year data with 1000 MW thermal power reactor for attaining statistics sufficiently for the analysis purpose. We implement a fit with five parameters, including a normalization factor α_0, fractional ratio of Pu isotopes α_1, fractional ratio of ^{239}Pu in the Pu isotopes α_2, fractional ratio of ^{235}U in the U isotopes α_3, and a normalized background parameter α_4. Assuming the nominal power-equal IBD event rates at the i-th. energy bin with four main isotopes ^{235}U, ^{238}U, ^{239}Pu, and ^{241}Pu are $N_{\text{ref.}}^{U-235,i}, N_{\text{ref.}}^{U-238,i}, N_{\text{ref.}}^{Pu-239,i}$, and $N_{\text{ref.}}^{Pu-241,i}$ respectively. Technically, we simulate these IBD rate with the 1:1:1:1 isotope composition. The total predicted number of the IBD-like events, including the signal and background, can be written as:

$$N_{\text{pred.}}^i = \alpha_0 \times [N_{\text{ref.}}^{U-235,i} \times (1-\alpha_1) \times \alpha_3 + N_{\text{ref.}}^{U-238,i} \times (1-\alpha_1) \times (1-\alpha_3)$$
$$+ N_{\text{ref.}}^{Pu-239,i} \times \alpha_1 \times \alpha_2 + N_{\text{ref.}}^{Pu-241,i} \times \alpha_1 \times (1-\alpha_2)] + \alpha_4. \tag{4}$$

For a given isotope composition, for example ^{235}U : ^{238}U : ^{239}Pu : ^{241}Pu = 4:1:4:1, we generate a fake data sample and retrieve the isotope composition by adopting the binned χ^2 method to estimate the statistical significance. The χ^2 function, a statistical measure of the difference between a predicted spectrum $N_{\text{pred.}}^i$ computed at a given set of parameters of interest and an observed spectrum $N_{\text{obs.}}^i$ (either real data or fake data), is defined as following

$$\chi^2 = \sum_i \frac{(N_{\text{pred.}}^i - N_{\text{obs.}}^i)^2}{N_{\text{pred.}}^i \cdot N_{\text{pred.}}^i}$$

where i is the energy bin index. The minimization of χ^2 function allows us to find the best-fit set of parameters to describe the data and to attain the parameter intervals at the given statistical significance.

We consider for two cases: (i) without the background and (ii) with the background. The former case study is to validate our framework to extract the isotope composition.
Fig. 4 present a case study with isotope composition ^{235}U : ^{238}U : ^{239}Pu : ^{241}Pu = 4:1:4:1 without including the background. The total prediction at the best-fit parameters agrees with the fake data and the best-fit fractional composition of the Plutonium isotopes is 50%, which agrees with an addition of 40% of ^{239}Pu and 10% of ^{241}Pu. The 2σ and 3σ C.L. contours of two parameters, particularly α_0 and α_1 on the right plot of the Fig. 4, are presented to give us the quantitative estimation of the fractional isotope composition.

Apparently background-free detector is extremely challenging for the ground-level neutrino-based reactor monitor. Simulating the background is also difficult since it depends on the particular infrastructure of the reactor. A practical approach for background estimation is to measure with reactor-off state. Here we assume that the background is energy-independent for simplification. And we investigate for various scenarios of the S/B ratio. Fig. 5 shows a fit trial where
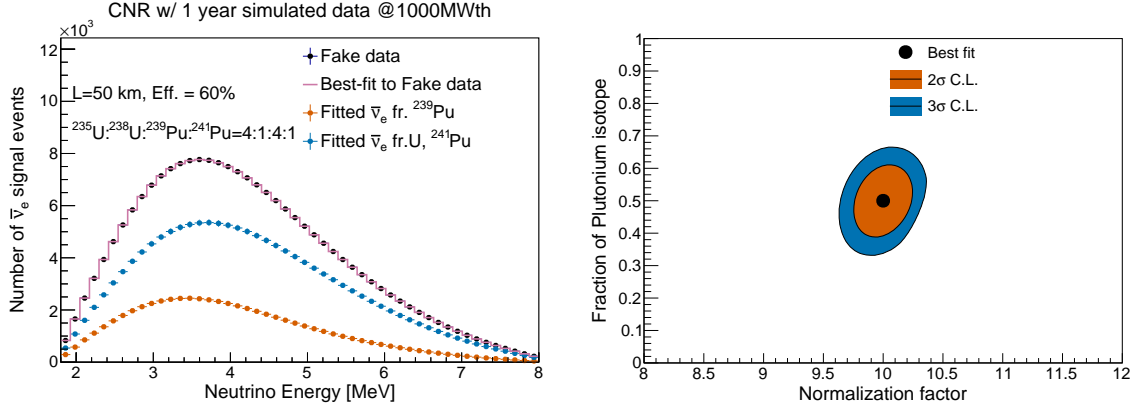
Fig. 4. (Color online) On the left plot, a fake data in black points is generated with an isotope composition assumed to be 4:1:4:1 and a 60% IBD detection efficiency. Background is assumed to be free. The total best-fit spectrum shown the purple, which is summed from best-fit spectrum of ^{239}Pu in the orange and the other contributions in the blue, agree well with fake data. The right plot show 2σ and 3σ C.L. contour of α_0 normalization factor and α_1 fractional content of Plutonium isotopes. The best-fit value of α_1 is 0.5, agree with an addition of 40% ^{239}Pu and 10% ^{241}Pu in the fake data.
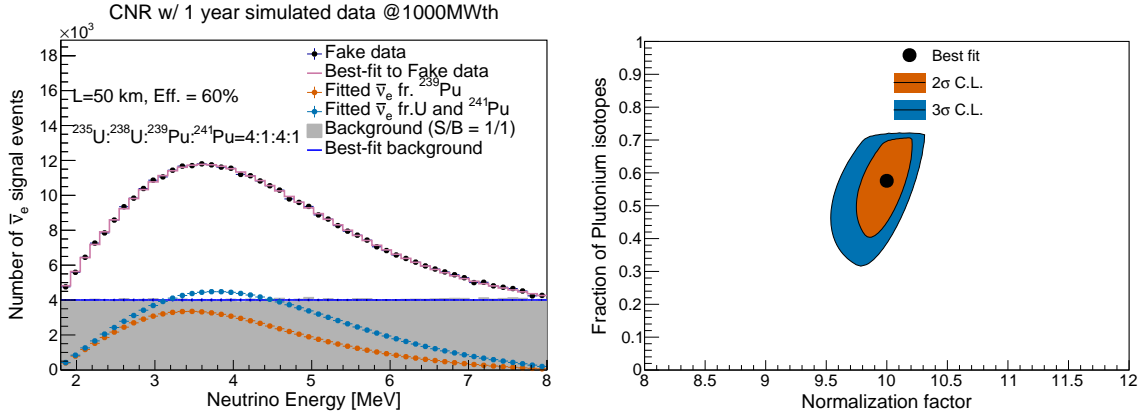

Fig. 5. (Color online) The experimental setup is similar to the scenario presented in Fig. 4 except that background is included with a S/B=1:1. Background events, presented in grey shaded histogram, are fluctuated based on the Poisson statistics. The total best-fit spectrum shown the purple, which is summed from best-fit spectrum of ^{239}Pu in the orange, the contributions from other isotopes in the blue, and background in the blue solid-line, agree with the data. The right plot shows 2σ and 3σ C.L. contours of α_0 normalization factor and α_1 fractional content of Plutonium isotopes. The best-fit value of α_1 is slightly deviation from the expected value 0.5, but agrees statistically with an addition of 40% ^{239}Pu and 10% ^{241}Pu in the fake data.

we assume the S/B to be 1:1, achieved with PROSPECT experiment [17], and the Poisson-based statistical fluctuation of the background events is applied for individual bins of energy. Overall the total best-fit spectrum, which is summed from the fitted IBD event rates from all isotopes

and a constant background rate, describes relatively well the fake data. The effect of the statistically fluctuated background is observable in the 2-dimensional contour of the normalization factor α_0 and the fraction of the Plutonium isotopes α_1. The best-fit value of α_1 is deviated from 0.5, which is expected as sum of 40% of ^{239}Pu and 10% ^{241}Pu, but still agrees within 2σ C.L. with the expectation. Another observable effect of the background is the enlargement and distortion of the 2-dimensional contour of the normalization factor and the fraction of Plutonium isotopes when compared to background-free case study in Fig. 4. To investigate the background fluctuation statistically, we typically generate 10^6 fake samples for each case of study by randomizing the background and fit independently. We then extract and accumulate the statistical distributions of the parameters of interest for the converged fit trials. The mean and root-mean-square (RMS) of the accumulated distribution are used to present the parameter of interest's central value and 1σ uncertainty.

In addition to the statistics of the observed IBD events, the precision of the extracted ^{239}Pu fractional content depends on the background level and reactor neutrino energy resolution. We investigate six experimental setups with two S/B levels (S/B=1:1 and S/B = 1:0.01) and three magnitudes of energy resolution (5%, 10%, and 15%). The accumulated distributions of the extracted ^{239}Pu fraction are shown in Fig. 6 and precision of the extraction, which is attained from the RMSs of the distributions, is presented in Table 6.
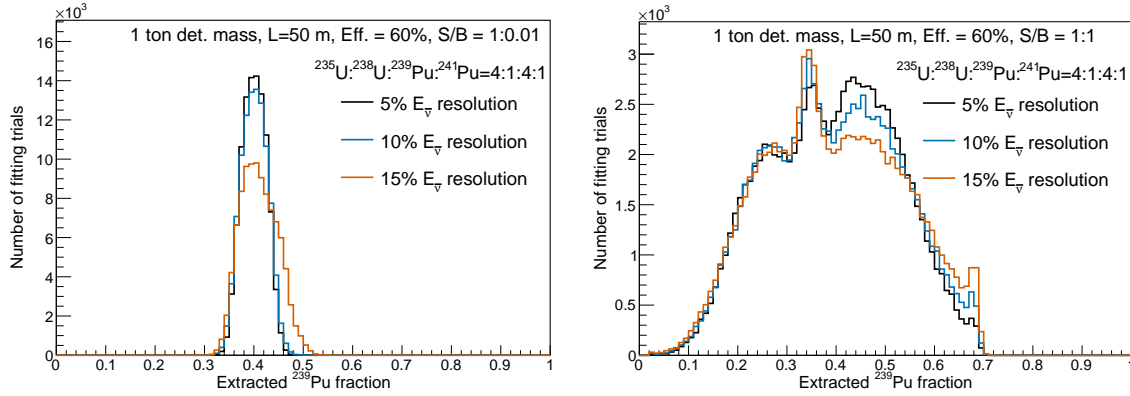

Fig. 6. Accumulated distributions of the extracted ^{239}Pu fraction with two S/B levels, S/B=1:0.01 (left) and S/B=1:1 (right), and three options of energy resolution (5%, 10%, and 15%). The fake data is generated for a 1-ton detector placed at 50 m from the reactor core with the isotope composition ^{235}U : ^{238}U : ^{239}Pu : ^{241}Pu = 4:1:4:1 with a 60% IBD detection efficiency. For each configuration, 10^6 fitting trials are performed on samples where Poisson-based randomized background events are included.

In case of the S/B=1:0.01, the precision of the extracted ^{239}Pu can range from 6.0% to 9.2%. The precision is less than 30% at the S/B = 1:1 level. The effect of energy resolution is visible, but the S/B level is the main driver for the precision of the extracted ^{239}Pu to reach few percent uncertainty, which is essential for tracking this weapon-usable isotope.

To investigate the potential of tracking ^{239}Pu fraction dynamically, we study three scenarios of isotope composition (i) ^{235}U : ^{238}U : ^{239}Pu : ^{241}Pu = 4:1:4:1, (ii) ^{235}U : ^{238}U : ^{239}Pu : ^{241}Pu

Table 6. Precision of the extracted ^{239}Pu fractional content, attained from the RMS of the accumulated distribution in Fig. 6, for two S/B levels, S/B=1:0.01 and S/B=1:1, and three options of energy resolution (5%, 10%, and 15%).

S/B ratio	Precision of the extracted ^{239}Pu		
	w/ 5% E_ν resol.	w/ 10% E_ν resol.	w/ 15% E_ν resol.
S/B=1:1	32.3%	33.4%	35.0%
S/B =1:0.01	6.0%	6.5%	9.2%

= 3:1:5:1, and (iii) ^{235}U : ^{238}U : ^{239}Pu : ^{241}Pu = 2:1:6:1, where the fractional content of ^{239}Pu varies from 40% to 60%. In Fig. 7, we show the precision of extracted ^{239}Pu fraction as a function of the background-to-signal ratio ranged from 1% to 100% with these three scenarios. We conclude that for a 1-ton detector placed 50 m away from the reactor core, the sensitivity to distinguish statistically the change in the three scenarios of the isotope composition is significant only when the background-to-signal is about 1%. However, if we increase the statistics by either using a larger detector or placing the detector closer to the reactor core, for example with a 10-ton detector mass placed at the 50 m standoff or a 1-ton detector mass at the 16 m standoff, the neutrino-based reactor monitor enables to tell distinctively the variation of ^{239}Pu from 40%, 50%, and 60% even with 10% level of the background-to-signal ratio.
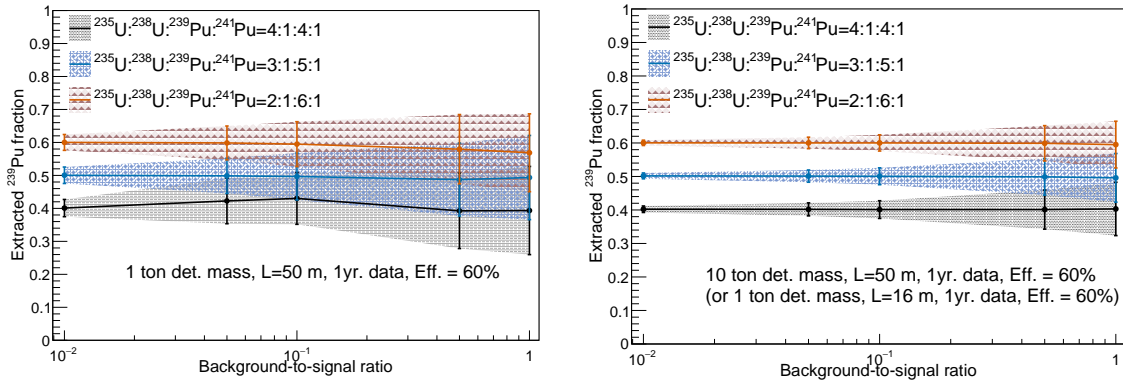

Fig. 7. The precision of extracted ^{239}Pu fraction as a function of the background-to-signal ratio ranged from 1% to 100% with three scenarios of the isotope composition: (i) ^{235}U : ^{238}U : ^{239}Pu : ^{241}Pu = 4:1:4:1, (ii) ^{235}U : ^{238}U : ^{239}Pu : ^{241}Pu = 3:1:5:1, and (iii) ^{235}U : ^{238}U : ^{239}Pu : ^{241}Pu = 2:1:6:1. The left is with a 1-ton detector mass placed at 50 m standoff. The right is with a 10-ton detector at the same standoff, which is statistically equivalent to a 1-ton detector placed at 16 m standoff.

6. Summary

The work is a preliminary investigation into using the neutrino-based reactor monitoring for safeguarding the reactors in Vietnam. The technique has been well-developed worldwide thank to the efforts from many reactor-based experiments. Our precise understanding of the reactor flux

and advantage in the neutrino detection technology allows us to have a nearly real-time and non-destructive reactor monitoring with reactor neutrinos. We simulated and computed the expected reactor neutrino rate and time to detect the reactor's on-off state transition for the on-going Dalat research nuclear reator (DNRR), the proposed 10 MW research facility (MPRR), and the considered 1000 MW commercial reactors (CNR). We report that, based on the current performance of neutrino detection technology, the expected IBD event rate is in the hundreds to thousands per year and that detecting the reactor's on-off state transition takes a few days to a month if the 1-ton detector is placed less than 20 m from the DNRR reactor core. The annual IBD event rate for the future MPRR and CNR facilities is expected to be 10^6, allowing us to detect the on-off transition of the reactor state in a matter of hours to days, even if the detector is placed 50 m away from the reactor core. Another focus of this study is on the possibility of extracting the fractional content of the nuclear weapon-usable ^{239}Pu isotope. We show that with the 100% background level, the 1-ton detector placed 50 m standoff can measure the ^{239}Pu fraction with a precision less than 30% and that a 1% background level is needed to differentiate the 10% variation of the ^{239}Pu fraction. The requirement for the background level can be loosened to 10% level if we can increase the statistics by having 10x larger detector or place detector $\sqrt{10}$ times closer to the reactor core.

Our work indicates that it is worthwhile to conduct research on the neutrino-based reactor monitor in Vietnam. While the technology as a whole is well-established around the world, more research into detection technology is needed to improve performance, lower costs, and make it more accessible. Our recent work with a novel type of silicon multiplier [56] demonstrates that this photosensor can be a good candidate for working with a plastic scintillator to build a monitor for this purpose, and our group plan to continue research in this area.

Acknowledgement

Authors contributions

All authors contributed equally to this work.

Conflict of interest

The authors have no conflict of interest to declare.

References

[1] W. Pauli, *Dear radioactive ladies and gentlemen*, *Phys. Today* **31N9** (1978) 27.

[2] F. Reines and C. L. Cowan, *The neutrino*, *Nature* **178** (1956) 446.

[3] M. Goldhaber, L. Grodzins and A. W. Sunyar, *Evidence for Circular Polarization of Bremsstrahlung Produced by Beta Rays*, *Phys. Rev.* **106** (1957) 826.

[4] T. Kajita, *Nobel lecture: Discovery of atmospheric neutrino oscillations*, *Rev. Mod. Phys.* **88** (Jul, 2016) 030501.

[5] A. B. McDonald, *Nobel lecture: The sudbury neutrino observatory: Observation of flavor change for solar neutrinos*, *Rev. Mod. Phys.* **88** (2016) 030502.

[6] PARTICLE DATA GROUP collaboration, P. A. Zyla *et al.*, *Review of Particle Physics*, *PTEP* **2020** (2020) 083C01.

[7] T2K collaboration, K. Abe *et al.*, *Constraint on the matter–antimatter symmetry-violating phase in neutrino oscillations*, *Nature* **580** (2020) 339, [1910.03887].

[8] M. S. Athar, S. W. Barwick, T. Brunner, J. Cao, M. Danilov, K. Inoue *et al.*, *Status and perspectives of neutrino physics*, *Prog. Part. Nucl. Phys.* (2022) 103947, [`arXiv:2111.07586`].

[9] T. Akindele, N. Bowden, R. Carr, A. J. Conant, M. Diwan, A. Erickson *et al.*, *Nu tools: Exploring practical roles for neutrinos in nuclear energy and security*, [`arXiv:2112.12593`].

[10] A. A. B. L. A. Mikaélyan, *Possibilities of the practical use of neutrinos*, *Atomic Energy* **44** (1978) 589.

[11] Y. V. K. V. I. K. L. A. M. et al., *Neutrino method remote measurement of reactor power and power output*, *Atomic Energy* **76** (1994) 123.

[12] B. Achkar, R. Aleksan, M. Avenier, G. Bagieu, J. Bouchez, R. Brissot *et al.*, *Search for neutrino oscillations at 15-meters, 40-meters, and 95-meters from a nuclear power reactor at Bugey*, *Nucl. Phys. B* **434** (1995) 503.

[13] A. Bernstein, Y.-f. Wang, G. Gratta and T. West, *Nuclear reactor safeguards and monitoring with anti-neutrino detectors*, *J. Appl. Phys.* **91** (2002) 4672, [`nucl-ex/0108001`].

[14] A. Bernstein, N. S. Bowden, A. Misner and T. Palmer, *Monitoring the Thermal Power of Nuclear Reactors with a Prototype Cubic Meter Antineutrino Detector*, *J. Appl. Phys.* **103** (2008) 074905, [`0804.4723`].

[15] H. Furuta, Y. Fukuda, T. Hara, T. Haruna, N. Ishihara, M. Ishitsuka *et al.*

[16] R. Carr *et al.*, *Neutrino-based tools for nuclear verification and diplomacy in North Korea*, *arXiv physics.soc-ph 1811.04737* (11, 2018) .

[17] PROSPECT collaboration, J. Ashenfelter *et al.*, *First search for short-baseline neutrino oscillations at HFIR with PROSPECT*, *Phys. Rev. Lett.* **121** (2018) 251802, [`1806.02784`].

[18] A. Bernstein, N. Bowden, B. L. Goldblum, P. Huber, I. Jovanovic and J. Mattingly, *Colloquium: Neutrino detectors as tools for nuclear security*, *Rev. Mod. Phys.* **92** (Mar, 2020) 011003.

[19] N. S. Bowden *et al.*, *Experimental results from an antineutrino detector for cooperative monitoring of nuclear reactors*, *Nucl. Instrum. Meth. A* **572** (2007) 985, [`physics/0612152`].

[20] D. Reyna, "A compact and portable antineutrino detector for reactor monitoring.." `https://www.osti.gov/biblio/1290207`, 2012.

[21] M. Battaglieri, R. De Vita, G. Firpo, P. Neuhold, M. Osipenko, D. Piombo *et al.*, *An anti-neutrino detector to monitor nuclear reactor's power and fuel composition*, *Nucl. Instrum. Meth. A* **617** (2010) 209.

[22] Y. Kuroda, S. Oguri, Y. Kato, R. Nakata, Y. Inoue, C. Ito *et al.*, *A mobile antineutrino detector with plastic scintillators*, *Nucl. Instrum. Meth. A* **690** (2012) 41, [`1206.6566`].

[23] NUCIFER collaboration, G. Boireau *et al.*, *Online Monitoring of the Osiris Reactor with the Nucifer Neutrino Detector*, *Phys. Rev. D* **93** (2016) 112006, [`1509.05610`].

[24] J. Carroll, J. Coleman, G. Davies, M. Lockwood, C. Metelko, R. Mills *et al.*, *Monitoring reactor anti-neutrinos using a plastic scintillator detector in a mobile laboratory*, [`1811.01006`].

[25] J. Coleman, C. Metelko, M. Murdoch, Y. Schnellbach, C. Touramanis, R. Mills *et al.*, *VIDARR: Aboveground Reactor Monitoring*, in *J. Phys. Conf. Ser.*, vol. 1216, p. 012007, 2019, DOI.

[26] R. Dorrill, *Nulat: A compact, segmented, mobile anti-neutrino detector*, in *J. Phys. Conf. Ser.*, vol. 1216, p. 012011, IOP Publishing, 2019.

[27] WATCHMAN collaboration, M. Askins, M. Bergevin, A. Bernstein, S. T. Dazeley, T. Dye, T. Handler *et al.*, *The physics and nuclear nonproliferation goals of WATCHMAN: A WAter CHerenkov Monitor for ANtineutrinos*, [`arXiv:1502.01132`].

[28] SoLid collaboration, Y. Abreu *et al.*, *Performance of a full scale prototype detector at the BR2 reactor for the SoLid experiment*, *JINST* **13** (2018) P05005, [`arXiv:1802.02884`].

[29] SoLid collaboration, Y. Abreu *et al.*, *SoLid: a short baseline reactor neutrino experiment*, *JINST* **16** (2021) P02025, [`arXiv:2002.05914`].

[30] I. Alekseev, V. Belov, V. Brudanin, M. Danilov, D. Egorov, D. Filosofov *et al.*, *Danss: Detector of the reactor antineutrino based on solid scintillator*, *Journal of Instrumentation* **11** (nov, 2016) P11011, [`1606.02896`].

[31] NEOS collaboration, Y. J. Ko *et al.*, *Sterile Neutrino Search at the NEOS Experiment*, *Phys. Rev. Lett.* **118** (2017) 121802, [`arXiv:1610.05134`].

[32] A. Haghighat, P. Huber, S. Li, J. M. Link, C. Mariani, J. Park *et al.*, *Observation of Reactor Antineutrinos with a Rapidly-Deployable Surface-Level Detector*, *Phys. Rev. Applied* **13** (2020) 034028, [`1812.02163`].

[33] H. Lima Jr *et al.*, *Neutrinos angra experiment: commissioning and first operational measurements*, *JINST* **14** (2019) P06010.

[34] STEREO collaboration, H. Almazán *et al.*, *Sterile Neutrino Constraints from the STEREO Experiment with 66 Days of Reactor-On Data*, *Phys. Rev. Lett.* **121** (2018) 161801, [`arXiv:1806.02096`].

[35] NEUTRINO-4 collaboration, A. P. Serebrov *et al.*, *First Observation of the Oscillation Effect in the Neutrino-4 Experiment on the Search for the Sterile Neutrino*, *Pisma Zh. Eksp. Teor. Fiz.* **109** (2019) 209, [`arXiv:1809.10561`].

[36] JUNO collaboration, F. An, G. An, Q. An, V. Antonelli, E. Baussan, J. Beacom *et al.*, *Neutrino Physics with JUNO*, *J. Phys. G: Nucl. Part. Phys.* **43** (2016) 030401, [`arXiv:1507.05613`].

[37] J. M. Berryman and P. Huber, *Sterile Neutrinos and the Global Reactor Antineutrino Dataset*, *JHEP* **01** (2021) 167, [`2005.01756`].

[38] M. Estienne, M. Fallot, A. Algora, J. Briz-Monago, V. M. Bui, S. Cormon *et al.*, *Updated summation model: An improved agreement with the daya bay antineutrino fluxes*, *Phys. Rev. Lett.* **123** (2019) 022502, [`arXiv:1904.09358`].

[39] P. Huber, "Neutrino science and nuclear security." https://doi.org/10.5281/zenodo.6683772, June, 2022. 10.5281/zenodo.6683772.

[40] P. Huber and T. Schwetz, *Precision spectroscopy with reactor antineutrinos*, *Phys. Rev. D* **70** (2004) 053011.

[41] K. Schreckenbach, H. Faust, F. von Feilitzsch, A. Hahn, K. Hawerkamp and J. Vuilleumier, *Absolute measurement of the beta spectrum from 235u fission as a basis for reactor antineutrino experiments*, *Phys. Lett. B* **99** (1981) 251.

[42] K. Schreckenbach, G. Colvin, W. Gelletly and F. Von Feilitzsch, *Determination of the antineutrino spectrum from 235u thermal neutron fission products up to 9.5 mev*, *Phys. Lett. B* **160** (1985) 325.

[43] A. A. Feilitzsch, F. von Hahn and K. Schreckenbach, *Experimental beta-spectra from 239pu and 235u thermal neutron fission products and their correlated antineutrino spectra*, *Phys. Lett. B* **118** (1982) 162.

[44] A. Hahn, K. Schreckenbach, W. Gelletly, F. von Feilitzsch, G. Colvin and B. Krusche, *Antineutrino spectra from 241pu and 239pu thermal neutron fission products*, *Phys. Lett. B* **218** (1989) 365.

[45] N. Haag, A. Gütlein, M. Hofmann, L. Oberauer, W. Potzel, K. Schreckenbach *et al.*, *Experimental Determination of the Antineutrino Spectrum of the Fission Products of* ^{238}U, *Phys. Rev. Lett.* **112** (2014) 122501, [`arXiv:1312.5601`].

[46] T. A. Mueller, D. Lhuillier, M. Fallot, A. Letourneau, S. Cormon, M. Fechner *et al.*, *Improved predictions of reactor antineutrino spectra*, *Phys. Rev. C* **83** (May, 2011) .

[47] P. Huber, *On the determination of anti-neutrino spectra from nuclear reactors*, *Phys. Rev. C* **84** (Aug, 2011) 024617.

[48] L. Hayen, J. Kostensalo, N. Severijns and J. Suhonen, *First-forbidden transitions in the reactor anomaly*, *Phys. Rev. C* **100** (2019) 054323, [`arXiv:1908.08302`].

[49] P. Vogel and J. F. Beacom, *Angular distribution of neutron inverse beta decay,* $\bar{\nu}_e + p \rightarrow e^+ + n$, *Phys. Rev. D* **60** (Jul, 1999) .

[50] N. D. Nguyen, B. V. Luong, V. V. Le, V. D. Duong, X. H. Nguyen, N. S. Pham *et al.*, *Results of operation and utilization of the Dalat Nuclear Research Reactor*, *Nuclear Science and Technology* **4** (Mar., 2014) 1.

[51] N.-D. Nguyen, K.-C. Nguyen, T.-N. Huynh, D.-H.-D. Vo and H.-N. Tran, *Conceptual design of a 10 mw multi-purpose research reactor using vvr-kn fuel*, *Science and Technology of Nuclear Installations* **2020** (Aug, 2020) 7972827.

[52] Q. B. Do, G. T. Phan, K.-C. Nguyen, Q. H. Ngo and H.-N. Tran, *Criticality and rod worth analysis of the dnrr research reactor using the srac and mcnp5 codes*, *Nuclear Engineering and Design* **343** (2019) 197.

[53] G. T. Phan, Q. B. Do, Q. H. Ngo, T. A. Tran and H.-N. Tran, *Application of differential evolution algorithm for fuel loading optimization of the dnrr research reactor*, *Nuclear Engineering and Design* **362** (2020) 110582.

[54] "Nuclear power in Vietnam." `https://world-nuclear.org`.

[55] P. Huber, M. Lindner and W. Winter, *Superbeams versus neutrino factories*, *Nucl. Phys.* **B645** (2002) 3, [`hep-ph/0204352`].

[56] N. H. D. Thanh, N. V. C. Lan, C. V. Son, T. V. Ngoc, P. T. Quyen, N. Khoa *et al.*, *Multi-pixel Photon Counter for operating the tabletop cosmic-ray detector under loosely controlled conditions*, [`arXiv:2106.08603`].